TRENDS IN SCIENCES 2025; 22(12): 10921
https://doi.org/10.48048/tis.2025.10921 RESEARCH ARTICLE

Investigation of the Influence of RF Plasma on the Properties of Spinel Ferrite $Mg_{1-X}Cu_xFe_2O_4$

Alyaa Hefdhi Abbas Aziz*, Ibtesam Omran Radi and Faten D. Mirjan

Department Physics, College of Science, University of Babylon, Hilla 51001, Iraq

(*Corresponding author's e-mail: sci.alyaa.hofdhy@uobabylon.edu.iq)

Received: 11 June 2025, Revised: 18 June 2025, Accepted: 25 June 2025, Published: 20 September 2025

Abstract

The current study attempts to enhance the process parameters of radiofrequency plasma technology. $Mg_{1-x}Cu_xFe_2O_4$ is synthesized making use of the sol-gel technique at various copper concentrations (x = 0, 0.3, 0.7). X-ray diffraction analysis confirms the presence of a face-centered cubic (FCC) architecture in ferrite samples. Particle sizes changed before plasma exposure and after increasing the copper concentration, with a slight decrease in size. After exposure, a decrease in particle size was also evident. FESEM analysis revealed that Mg Fe_2O_4 particles were nearly spherical, whereas $CuFe_2O_4$ particles were rod-shaped, showing that Cu doping increased morphological anisotropy. Copper ferrite ($Mg1\text{-}xCu_xFe_2O_4$) exhibits a large crystal size. Exposure to plasma alters the crystal's shape and size significantly, resulting in a heterogeneous and non-spherical structure. VSM tests show that soft ferritic materials exhibit a tiny magnetic residual loop. Prior to plasma treatment, the magnetic saturation magnetization of $Mg_{1-x}Cu_xFe_2O_4$ fluctuated to increases when the ratio (x) increased owing to crystalline magnetism differences. Exposure to plasma increased the Ms (magnetic saturation) value of $Mg_{1-x}Cu_xFe_2O_4$, while the Mr (residual magnetism) value of unexposed samples increased with copper concentration in ferrites. The variance is described in terms of cationic distribution, ferrite tetragonality, and the Néel 2-sub-lattice concept (The Néel 2-sublattice idea depicts antiferromagnetic by dividing a magnetic material's atomic spins into 2 interpenetrating sublattices, each with its own magnetic moment. These sub lattices are organised in such a way that the magnetic moments on each sublattice align in opposing directions, resulting in zero net magnetization).

Keywords: RF Plasma, Sol-gel Scherrer's equation, VSM measurements, FESEM tests, Coercive force, Saturation magnetization

Introduction

Ferrites with spinel structures are critical components for soft magnetic and solid-state microwave applications. The intrinsic properties of the material as well as the influence of grain sizes determine the suitability of particular materials [1]. Typically, ferrites are non-conductive ferrimagnetic ceramic compound materials with the chemical formula AB_2O_4, which combine 2 magnetic ions and oxygen to create spontaneous magnetisation, where the tetrahedral and octahedral cation positions in an FCC anion (oxygen) sublattice are denoted by (A) and (B), respectively [2,3]. The chemical classes oxides, germinates, and silicates make up the spinel group. The minerals that make up the iron-spinel (spinel ferrite) series are hard, dark black to

brownish, and have little coercivity [4]. Because polycrystalline ferrites are excellent dielectric materials, they may be used in microwave and radio frequency applications. These materials' high permeability and low electrical conductivity make them ideal for switch mode power supplies, transformer cores, and inductors [5]. These spinels are found in high-temperature sulphide veins, stony meteorites, and igneous, metamorphic granite pegmatites as masses [6]. An inverse spinel known as cuprospinel ($CuFe_2O_4$) occurs when Copper takes the

place of some of the iron cations in the structure. Copper ferrite, another name for cuprospinel, resembles magnetite in structure [7].

Cuprospinel is primarily composed of 2 elements: Iron (Fe^{2+} and Fe^{3+}) that break apart tetrahedral sites and copper (Cu^{2}) that occupies octahedral sites. $Iron^{+2}$ and $iron^{+3}$ occupy a number of octahedral and several tetrahedral sites, The role of Fe^{3+} ions in influencing the structural and magnetic behavior of spinel ferrites was discussed in our previous study [8]. The cooperative Jahn-Teller effect causes a structural phase change when Cu is substituted, which is followed by a decrease in crystal symmetry [9]. On the other hand, $MgCu_xFe_2O_4$ is an n-type semiconducting material with a soft magnetic property. Numerous physical and chemical characteristics of $MgCu_xFe_2O_4$ are dependent on the cation distribution, which is a complicated function of processing factors primarily determined by the material's manufacturing technique [10]. The cation distribution that was previously described indicates that although Mg^{2+} ions are present in both locations, they strongly favour the octahedral site [11]. Our goal is to examine the magnetic and structural characteristics of Cu-Mg, inspired through the electrical, structural, and dielectric components, conductivity investigations of Cu Fe_2O_4 ferrites made using different techniques. These materials' exposure to high temperatures may cause structural and magnetic surface abnormalities, which would clarify the intriguing. Using a chemical process called "sol-gel", materials are created by changing from a liquid phase (sol) to a solid phase (gel)[12]. When this technology is used in fabrication, the spin-coating or dip-coating procedure is often followed by the heat-treatment process, Dwi Teguh Rahardjo and et al. also manufactured ferrite and also by the sol-gel method and studied the magnetic and structural properties. [13]. When plasma and treated surfaces come together, they can produce a covering, a high-tensile layer that leads to connecting, coating, and printing. They can also make a rough pattern, build a dense interlocking layer, an object alteration and a chemical response with additional ingredients. Therefore, an attempt has been made to investigate the structural and magnetic properties of sol-gel-prepared magnesium-doped copper ferrite in the current work and effect the RF plasma of this material to prepare it, Farheen and Singh studied effect the plasma [14].

Materials and methods

Materials

In this experiment, Cooper Nitrate Hexahydrate ($Cu(NO_3)_2.3H_2O$),Hexahydrate of magnesium nitrate ($Mg(No_3)_2.6H_2O$), ferric nitrate nanohydrate ($Fe(NO_3)_3.9H_2O$),, and citric acid ($C_6H_8O_7.H_2O$)and Ammonium Hydroxide (NH4OH) were employed for preparing the samples. The samples were created by combining the mixtures together. The necessary supplies were used as provided.

Synthesis

The first in work, the masses are calculated as the primary mass, where the proportions of the components of one mole are determined in terms of the atomic weights for each element, and according to the relationship, the **Table 1** show the weights used in preparing ferrite compounds.

n = W / Wm

(n): Number of moles.
(W): Weight to be calculated for the preparation of the samples.
(Wm): Molecular weight.

Our goal with the sol-gel method is to create a homogenous precursor solution. For this, a homogenous solution is first obtained by mixing the precursor and the solvent (which typically consists of water, organic solvents, or a combination of them) in a heat-resistant container size (500 mL).

Table 1 Displays the pure material shows the weights that were used to make the composite $Mg_{1-x}Cu_x Fe_2O_4$.

No. of mole	$Fe(NO_3)_3.9H_2O$	$Cu(NO_3)_2.3H_2O$	$C_6H_8O_7$	X	1-X	$2Fe(NO)_3.9H_2O$	$Mg(No_3)_2.6H_2O$
1	404.0	241.60	192.12			808	256.41
0.1	404	24.160	19.212	0	1	808	25.641
	40.4	0					25.641
		7.248		0.3	0.7	80.8	17.948
		16.91		0.7	0.3		7.692

Afterwards, place the mixture on a magnetic mixer (magnetic stirring) until it reaches a temperature of 60 °C and becomes homogenous (all raw components have melted completely). The procedure known as sol-gel typically converts sol to gel by altering the pH or concentration of the solution by adding ammonia to alter the pH of the mixture so that it is (pH > 7). It will rise temperature is gradually to 60 °C for 2 h. The temperature of the solution will continue to gradually rise until it reaches 90 °C for 15 min, then raises the temperature again to 110 °C, where the gel begins to turn into a dry gel where the top surface of the gel is a coherent surface. **Figure 1**. When the temperature rises over 120 °C, the dry gel begins to self-combust. As seen in **Figure 1(A)**, the gel assumes a loose structure after the combustion is complete. It then cools and is ground to powder. It is sintered for 2 h at 1,100 °C after being put back in the convection oven.

After that, it is allowed to cool in the oven for 24 h. The powder was then compressed using a hydraulic press at 150 kN of pressure for 2 min, forming it into a 20 mm diameter disc, as seen in **Figure 2**.

Plasma exposure

The sample is displayed to the plasma using the RF system. It took 2 h to expose each sample inside the system. Then compare the results before and after exposure to plasma and study the effect of plasma on the properties of the prepared material. The samples are then added to the RF magnetron sputtering apparatus; **Figure 3** displays the components of the RF sputtering system utilised in this investigation. It was submitted via the following 3 primary methods: We closed the cap after cleaning the brass target and positioning the spotless substrates at the sample step in the centre of a chamber.

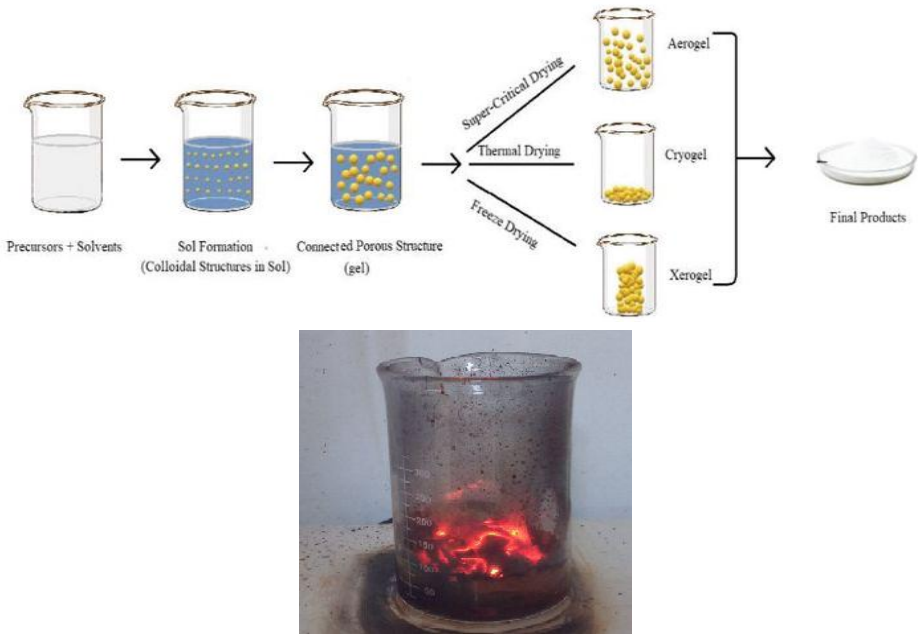

Figure 1 Gel production in various forms using the sol-gel technique and, A is Burnt ferrite

Figure 2 Samples disc.

Activate the rotating vacuum and raise the temperature to 523 K. Once the necessary pressure is reached, the gadget is activated. For the most productive plasma creation, the space inside has to be filled with the gas argon. Then, the RF source must be turned on, and the refraction power must be reduced until it approaches 0. At this point, the deposit process kicks off, and it takes 2 h to complete.

Figure 3 Composition of RF magnetron sputtering system.

Results and discussion

Field emission scanning electron microscope test (FE-SEM)

Solids', molecules', and nanomaterials' chemical and physical characteristics are influenced by the spatial organisation of ions and the distribution of electrons [15]. **Figures 4(a) - 4(C)** displays the FE-SEM micrographs at various magnifications and the EDS analysis pertaining to $Mg_{1-x}C_xFe_2O_4$ nanoparticles. It is evident that the particles have a mainly spherical shape and are less than 100 nm in size. correspondingly, which displays the particle morphologies with the copper ferrite crystal size span from (39.14) nm. Despite the fact that the magnesium frit's crystal size is (40.43) nm, it can be seen that magnesium ferrite's crystal size is bigger than copper ferrite's due to the magnesium ion's higher ionic radius. The particles differed from each other in size before plasma exposure in FE-SEM micrographs; it shows that the grains have a non-uniform grain size distribution. The copper ion at the surface of the tetrahedral site causes a reduction in the size of the nanoparticles; that is, a particle rate decreases as the copper ion (Mg^2) is replaced by the magnesium ion (Cu^2) in the crystal lattice. The results of the XRD examination matched the results obtained from the FE-SEM examination by M Ansari *et al.* [16].

The surface of the compound heterojunction has a homogeneous distribution of magnesium, copper, and oxygen. It shows that these components are strongly supporting an effective ion-exchange procedure, as **Figures 5(a) - 5(c)** show the change in the size and

shape of the sample after exposure to the plasma. In terms of size, the ferrite magnesium crystal is rather large. However, when the concentration of copper ions increased, a decrease in the particle size was also observed. We noticed a significant change in the shape and size of the crystal. The plasma contains positive ions, electrons, and atoms. All of these components can interact with the surface during the plasma treatment, by studied by A.H Abbas *et al.* [17] when morphological studies demonstrated uneven grain distribution and dominating aggregation in ferrite before and after treatment.

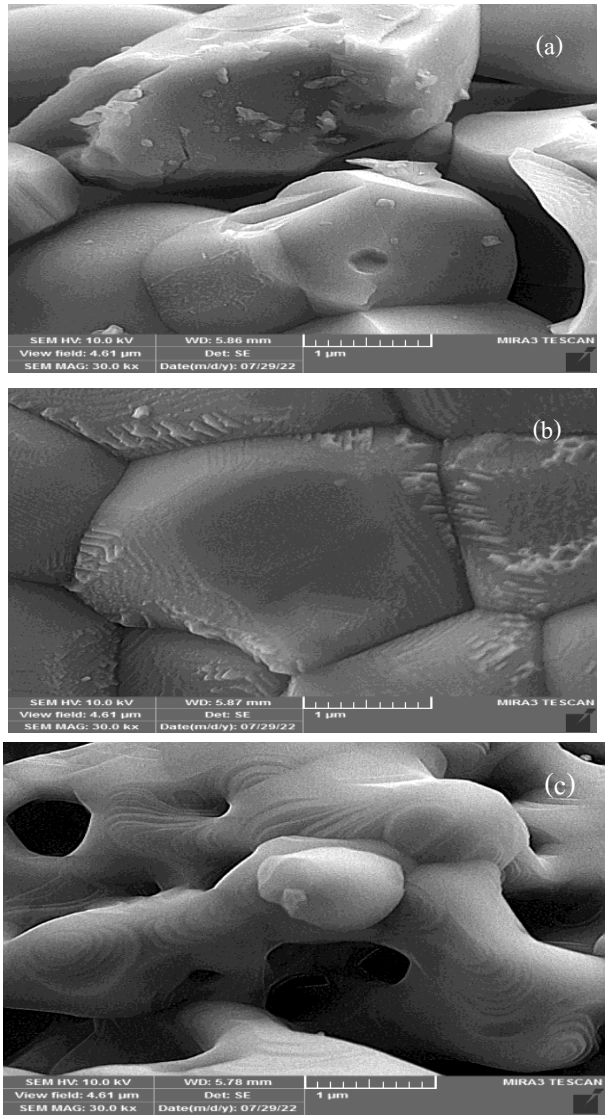

Figure 4 FESEM images of compound $Mg_{1-x}Cu_xFe_2O_4$ at ratio (a) x = 0, (b)x = 0.3, (c) x = 0.7 before plasma exposure.

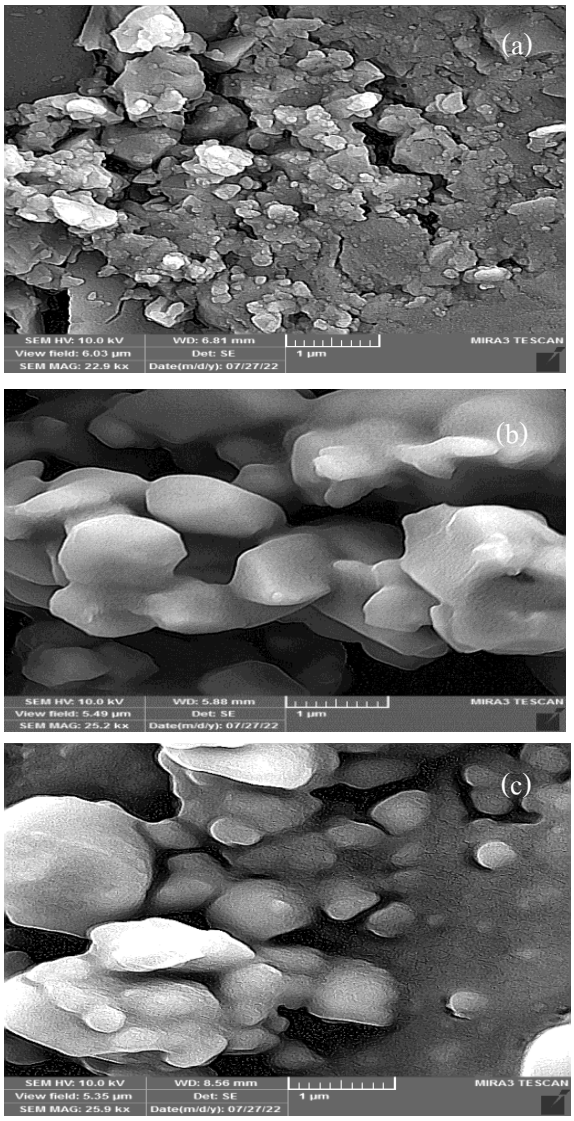

Figure 5 FE-SEM images of compound $Mg_{1-x}Cu_xFe_2O_4$ at ratio (a)x = 0, (b) x = 0.3, (c) x = 0.7 after plasma exposure.

Study analysis of X-ray diffraction (XRD)

The various phases and structural characteristics of the powdered $Mg_{1-x}Cu_xFe_2O_4$ samples were investigated using an XRD instrument. The X'Pert High Score Plus is employed to plot the results in the form of peak intensity on the y-axis and the measured diffraction angle on the x-axis. At each peak that is in a diffraction pattern formed because the X-ray beam is diffracted from the plane in the sample material. Therefore, each peak has a mutually proportional intensity and number of X-ray photons that can be detected by detectors at each angle. The produced ferrite's crystal structure and synthetic data were confirmed using an X' Pert PW 3040/60 diffractometer (λ = 1.54). The generated material's results may be compared to the International Centre of Diffraction Data (ICDD) to diagnose the material using the X-ray diffraction diagram.

Evidently, the face-centred cubic (FCC) structure may be indexed to $MgFe_2O_4$ (ICSD Card No.01-088-1937) [17]. The XRD spectra of the compound $Mg_{1-x}Cu_xFe_2O_4$ are shown in **Figures 6(a) - 6(c)**. Examining further, diffraction peaks are seen at the crystal planes (220), (311), (400), (511) and (440), as shown in **Figures 4(a) - 4(b)**. These peaks verify that all of the produced $Mg_{1-x}Cu_xFe_2O_4$ samples include a face-centred cubic (FCC) spinel phase. These doped samples don't exhibit any signs of secondary phases, proving the product's great purity of the cubic spinel structure even at different ratios of Cu^{2+} concentrations. The common pattern of crystallisation development (311) from 2θ = 35.8° to 35.5° indicates a reduction in

the crystalline frit of magnesium as the distance between the peaks grows and reduces based on the concentration of Cu^{+2} by Hammad *et al.* [18] demonstrated that the size of the crystallite as measured by XRD data and the particle size acquired are compatible. Prior to plasma exposure, structural data are displayed in **Table 2** when hkl (Miller transactions), FWHM (full width at half maximum), Spacing between crystal planes (dhkl) and lattice constant (a) and D the granular size is determined by applying the Scherrer equation found in Eq. (1) [19]. The formula in question includes a constant (k) called the form factor, β representing the full-width half optimum, θ representing Bragg's diffraction angle, and λ representing the X-ray wavelength (1.545 nm).

$$D = K \lambda / (\beta \cos \theta) \quad (1)$$

Prior to plasma exposure, an increase in copper ion concentration causes the crystal structure's pressure to rise, which reduces the size of the nanoscale crystallites. This is because, when the copper ion is substituted with magnesium ions, the particle size falls because the magnesium ions' ionic radius (0.75) nm is bigger than the copper ion's (0.73) nm, studied by A.H Abbas *et al.* [19] When samples exposed to plasma were found to possess a structure of cubic spinel and display irregular structural parameter fluctuation with exposure, X-ray measurements.

A peak (422) emerged after the samples were exposed to plasma, and the general trend of crystal development stayed at (311), with the strength of the peak decreasing at most concentrations compared to before the samples were exposed to plasma. The diffraction peaks decreased in strength but stayed the same following exposure, as seen in **Figure 7**. Additionally, following plasma exposure, it was observed that the crystal size (D) shrank as the concentration of Cu increased **Table 3**. When the concentration of copper ions was raised, significantly fewer peaks were observed in the samples' X-ray observations following their exposure to plasma, studied by M Desai *et al.* [20]. The current X-ray analysis revealed the presence of nanocrystalline grains in the lithium zinc ferrite thin films.

Table 2 Structural properties of compound Mg_{1-x} $Cu_xFe_2O_4$ prior to exposure to plasma.

The component	(hkl)	Peak-position (2θ)	FWHM	Crystallite D's size (nm)	d_{hkl} (nm)	a(Å)
$Mg_{1-x}Fe_2O_4$	311	36.8	0.12	54.9	2.52	8.743
$Mg_{0.7}Cu_{0.3}Fe_2O_4$	311	36.59	0.12	55.1	2.58	8.73
$Mg_{0.3}Cu_{0.7}Fe_2O_4$	311	34.51	0.16	39.6	2.53	8.75

Table 3 Structural properties of compound $Mg_{1-x}Cu_xFe_2O_4$ after to exposure to plasma.

The component	(hkl)	Peak-Position (2theta)	FWHM	Crystallite D's size (nm)	d_{hkl} (nm)	a(Å)
$Mg_{1-x}Fe_2O_4$	311	35.6	0.12	54.7	2.50	8.72
$Mg_{0.7}Cu_{0.3}Fe_2O_4$	311	35.5	0.13	51.5	2.53	8.71
$Mg_{0.3}Cu_{0.7}Fe_2O_4$	311	35.51	0.16	37.9	2.52	8.76

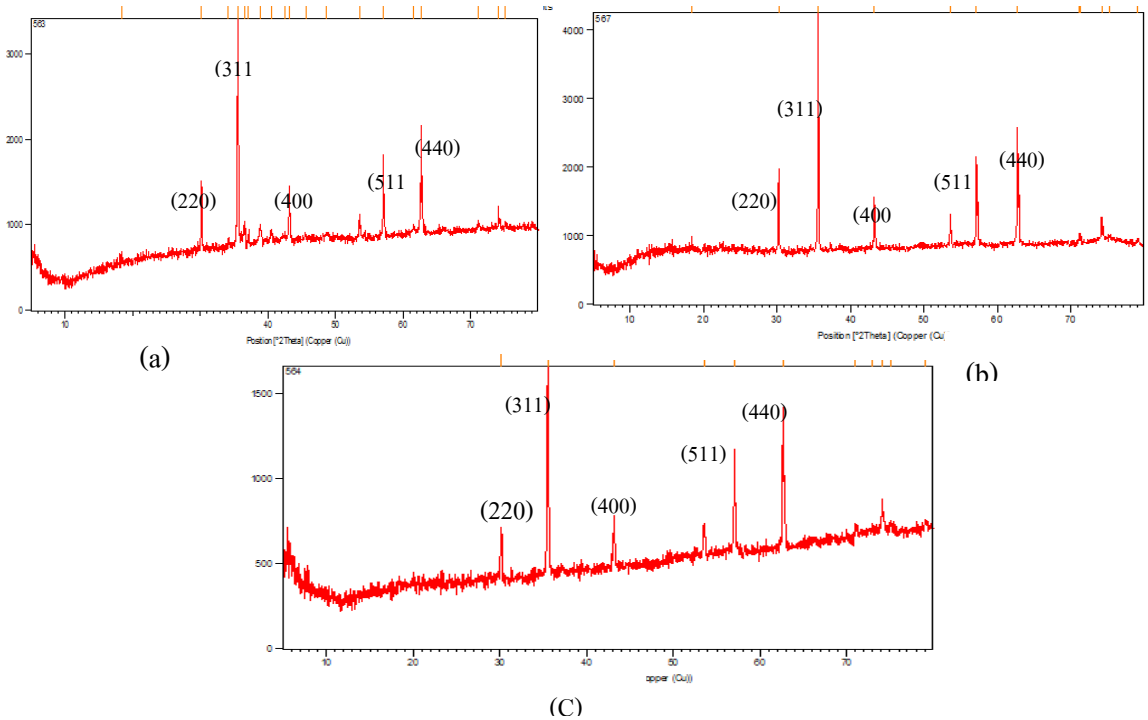

Figure 6 X-ray patterns of $Mg_{1-x}Cu_xFe_2O_4$ using varied Mg ratios at (a) x = 0, (b) x = 0.3, (c) x = 0.7 before plasma exposure.

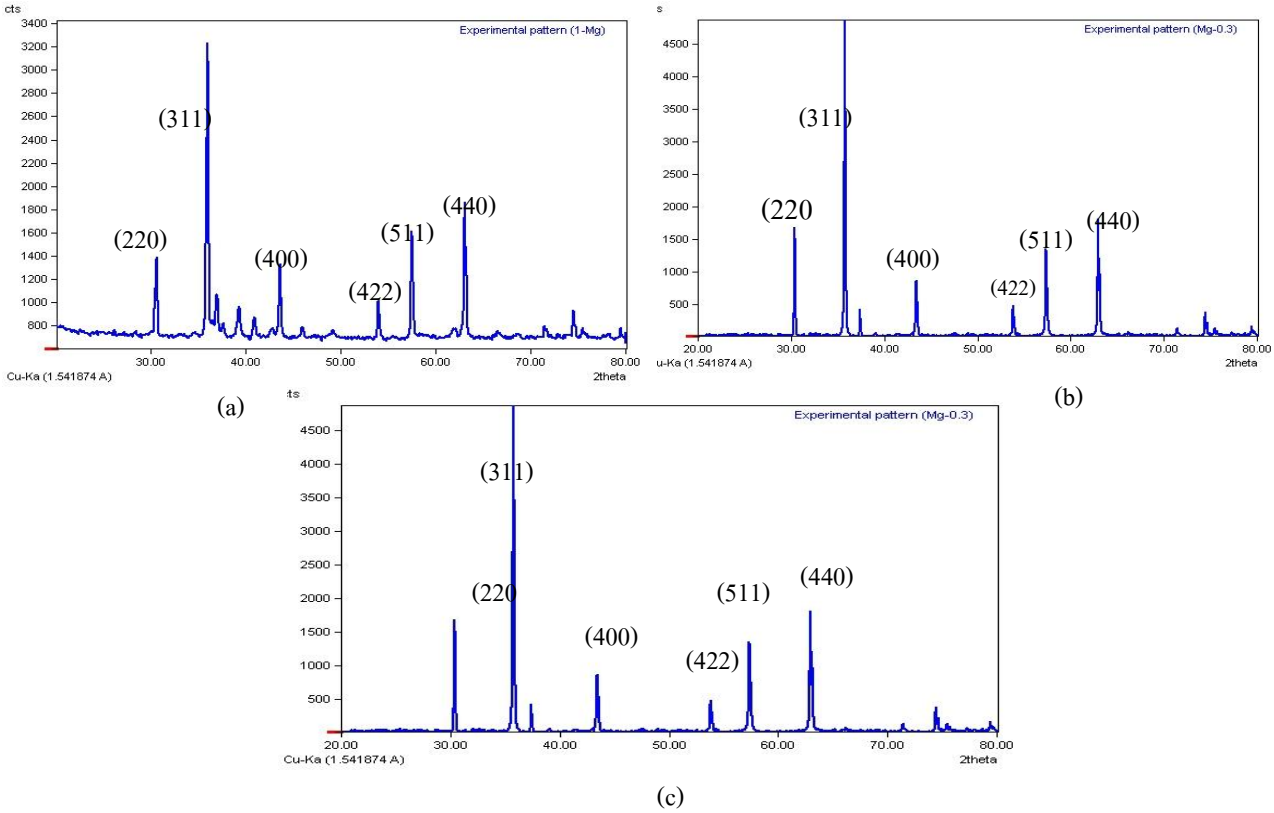

Figure 7 X-ray patterns of $Mg_{1-x}Cu_xFe_2O_4$ using varied Mg ratios at (a) x = 0, (b) x = 0.3, (c) x = 0.7 after plasma.

Magnetic data

A vibration sample magnetometer (VSM) at room temperature is employed to examine the magnetic properties of the produced both the intensity of the magnetic field and the specimens. Using the concept of magnetic hysteresis, researchers can get insight into the magnetic behaviour of samples and learn more about specific magnetic variables [21]. Seen in various sections are the material's magnetic characteristics. In part (a) the hysteresis curve has a nearly symmetrical reverse sequence when subjected to a magnetic field or when the magnetic field is removed. This is due to the very small amount of magnetic mineral content in the sample. The hysteresis loop of $Mg_{1-x}Cu_xFe_2O_4$ ferrite is depicted in **Figures 8(a) - 8(c)** before plasma exposure, which provides insight into the samples' magnetic behaviour. The magnetic characteristics with ferrite spinel behaviour are shown by the thin curves. This is the property of soft ferrite, a substance that loses its magnetism. The composite's magnetic behaviour at x = (0, 0.3, 0.7) is depicted in the image, along with magnetic parameters including coercive force (Hc), residual magnetisation (Mr), and saturation magnetism (Ms), where the area of the hysteretic loop decreases as the Cu^{2+} ion concentration rises. The **Table 4** clearly shows that the replacement of Cu causes a continuous fluctuation in magnetisation values, which enhances to a greater extent than saturated magnetisationM_S values. This might be due to the configuration of Cu^{+2} ions in cube-like structures and an increase in the residual magnetisation Mr ratio in the (x) ratio, as shown in **Figure 8(a)** Hammad's Lab researcher examined the same characteristics and discovered that as Ni^{2+} replaces (Cu^2), both saturation magnetisation and remanent magnetisation increase steadily [21]. This is related to particle size and shape, as well as the distribution of positive ions in the tetrahedral and octahedral structures. The stay in coercion might be related to the variance in crystal magnetism, studied by Mounkachi *et al.* [22] studied the magnetic exchange energies, inter- and intra-sublattices in $Mg_xCu_{-x}Fe_2O_4$ spinel for varied Mg concentrations ($0 \leq x \leq 1$) have been calculated.

After exposure to plasma, the morphologies revealed that they correlate to the natural behaviour, as shown in **Figures 9(a) - 9(c)**, with all rings confirming copper-magnesium ferroelectric soft magnetism. The thin hysteretic ring suggests a loss of magnetism. The magnetic characteristics of spinel ferrite are influenced by a number of parameters, including the process of synthesis, cation distribution on the tetrahedral and octahedral locations, and the increase in crystal size in relation to x. In **Table 5**, the magnetic properties were computed with the hysteresis looping process. It is obvious the table indicates that there was exposure to plasma causing the reduction and rise in the saturation area of the ratio of (x) samples that were not subjected.

Table 4 demonstrates the relationship(x) between the Cu^{+2} ratio and saturation of magnetic fields (Ms), remnant magnetism (Mr), and force coercive (Hc) prior to exposure to plasma.

Ratio(x)	The component	Ms emu/g	Mr emu/g	Hc Oe
0	$Mg_{1-x}Fe_2O_4$	22.0	1.9	25
0.3	$Mg_{0.7}Cu_{0.3}Fe_2O_4$	24.5	3.3	26
0.7	$Mg_{0.3}Cu_{0.7}Fe_2O_4$	27.6	2.9	29

Table 5 demonstrates the relationship(x) between the Cu^{+2} ratio and saturation of magnetic fields (Ms), remnant magnetism (Mr), and force coercive (Hc) during to exposure to plasma.

Ratio(x)	The component	Ms emu/g	Mr emu/g	Hc Oe
0	$Mg_{1-x}Fe_2O_4$	22.5	2.7	25
0.3	$Mg_{0.7}Cu_{0.3}Fe_2O_4$	24.9	3.04	25,5
0.7	$Mg_{0.3}Cu_{0.7}Fe_2O_4$	31.6	2.09	7.8

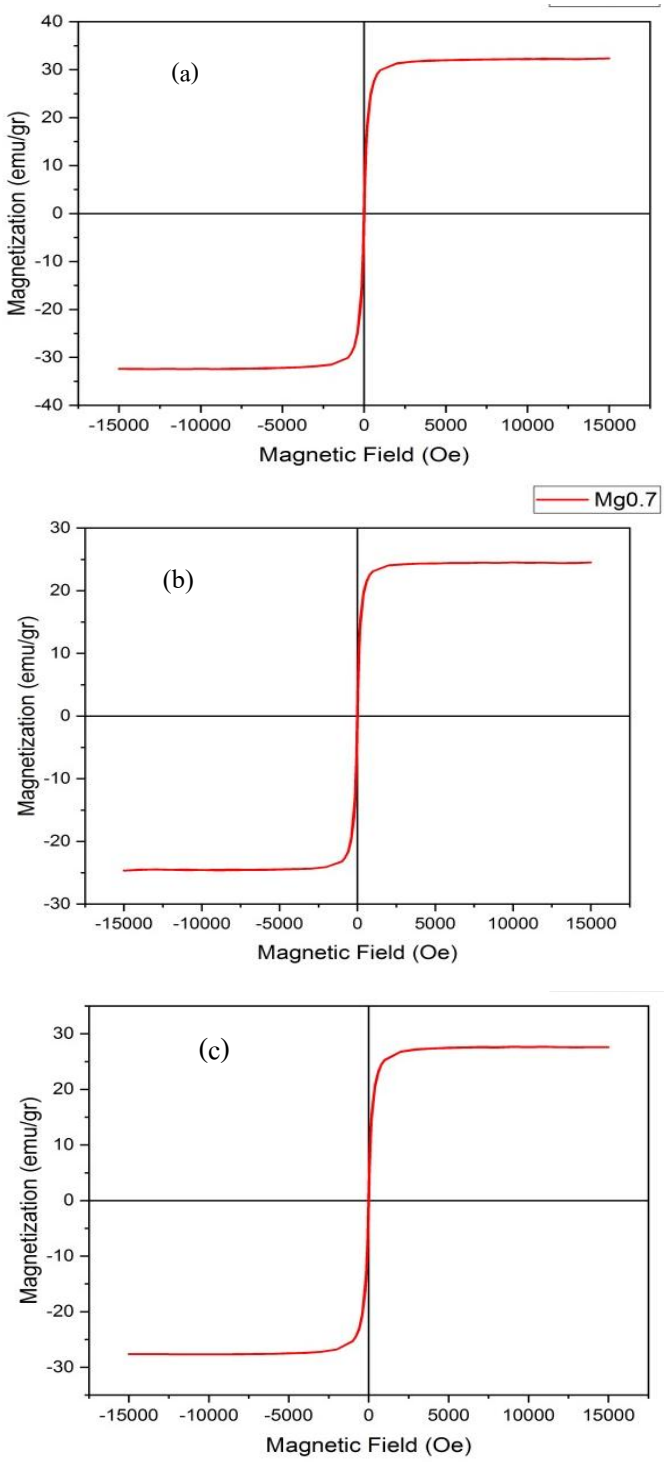

Figure 8 Magnetic curves of hysteresis of $Mg_{1-x}Cu_xFe_2O_4$ at (a) x = 0, (b) x = 0.3, (c) x = 0.7 before plasma exposure.

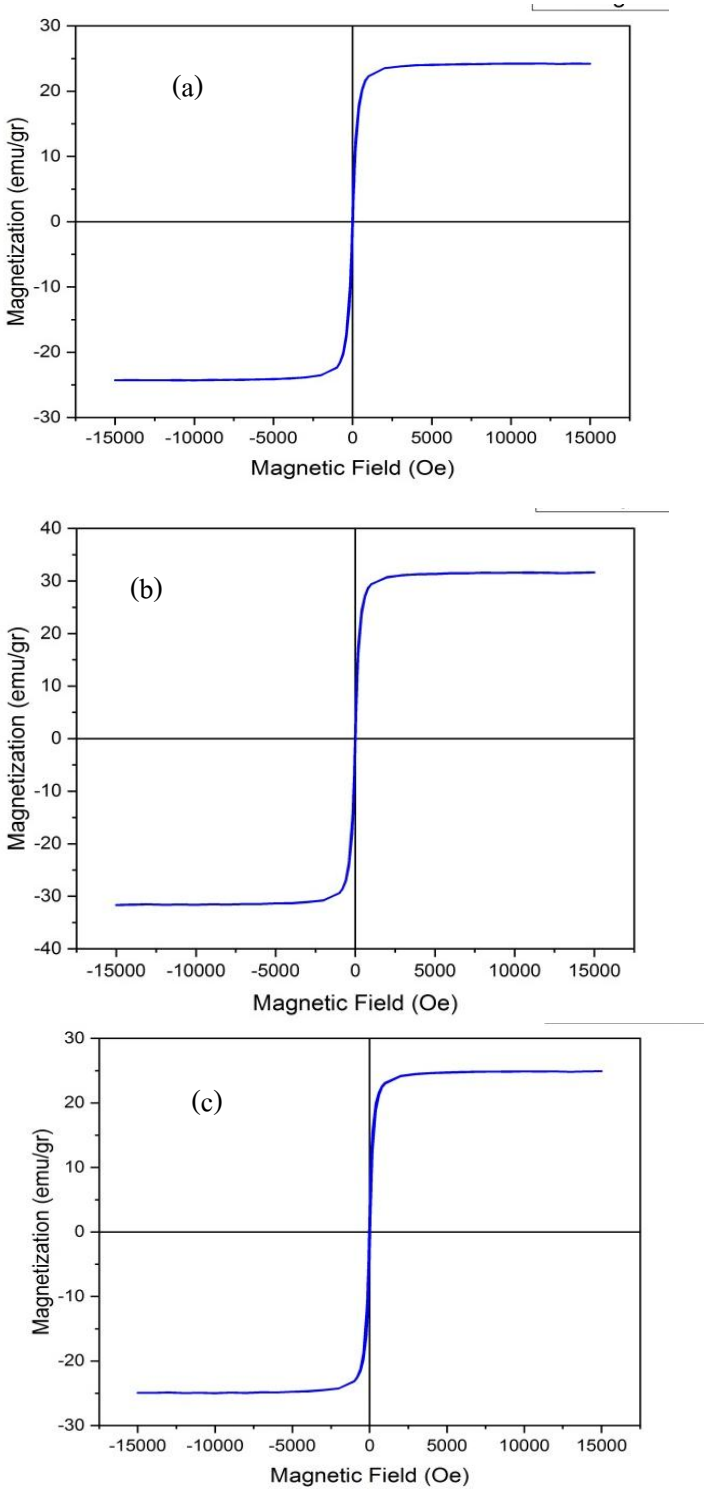

Figure 9 Magnetic curves of hysteresis of $Mg_{1-x}Cu_xFe_2O_4$ at (a) x = 0, (b) x = 0.3, (c) x = 0.7 after plasma exposure.

The same applies to values in Mr. and Hc, and a rise in Ms is seen in the plasma-treated ferrite cases [23]. This increase in saturation magnetisation is associated with the direct interaction of ferrite specimens using microwave plasma. Do not alter the value of the compulsion during plasma exposure [24].

Analysis (FTIR)

This experiment is a great way to demonstrate the characteristics and properties of materials as well as to investigate the distribution of cations in tetrahedral and octahedral sites in the ferrite system. where the ambient temperature FTIR spectra in the 400 - 4,000

cm^{-1} frequency band are displayed in **Figures 10** and **11**. The image makes it evident that each of the 2 samples' infrared spectra show 2 prominent absorption bands. The low-frequency band is associated with octahedral complexes, whereas the high-frequency band is associated with tetrahedral sites.

The compound $Mg_{1-x}Cu_xFe_2O_4$ infrared spectrum is displayed in **Figures 10(a) - 10(c)** for values of x = 0, 0.3, 0.7. The FTIR spectrum between (561 - 575) cm^{-1} revealed a number of bonds. It was evident from the results that this increase in the copper ratio caused a more red displacement than that of the magnesium ion because copper has the capacity to absorb or push the surrounding electronic densities equitably and because its radius is smaller than that of magnesium, it was clear from the results Fang *et al.* [25]. The FTIR and Cu spectra showed the symmetric and asymmetric vibrations of –CO-O- are shown by peaks at 1,563 and 1,450 cm^{-1}. Two absorption bands at (576.31 - 422.34) cm^{-1} are visible in the infrared spectra **Figures 11(a) - 11(c)** for all models following exposure of the same compound $Mg_{1-x}Cu_xFe_2O_4$ to the plasma. These band sites show the presence of (Cu^2) ions in the octahedral sites and Fe^{3+} ions in the tetrahedral sites. It was discovered that as the Mg^{2+} ion concentration rises, the band changes towards higher frequencies. This is seen at concentrations (x = 0, 0.6 and 1) where the infrared spectra (570.75 - 1,126.17) cm^{-1} appear following plasma exposure. The broadest peak is located close to where the stretching vibration of O=H groups originated. A higher concentration of free carriers and various flaws are linked to the OH peak at about 1,126.37 cm^{-1} from the results of Ramadan and El-MasryBarka [26], where explained, the addition of Zn to $CuFe_2O_4$results in a fairly constant (412 cm^{-1}) absorption band in FTIR spectra, representing stretching vibrations along the [MetalO] bond at the octahedral (B) position.

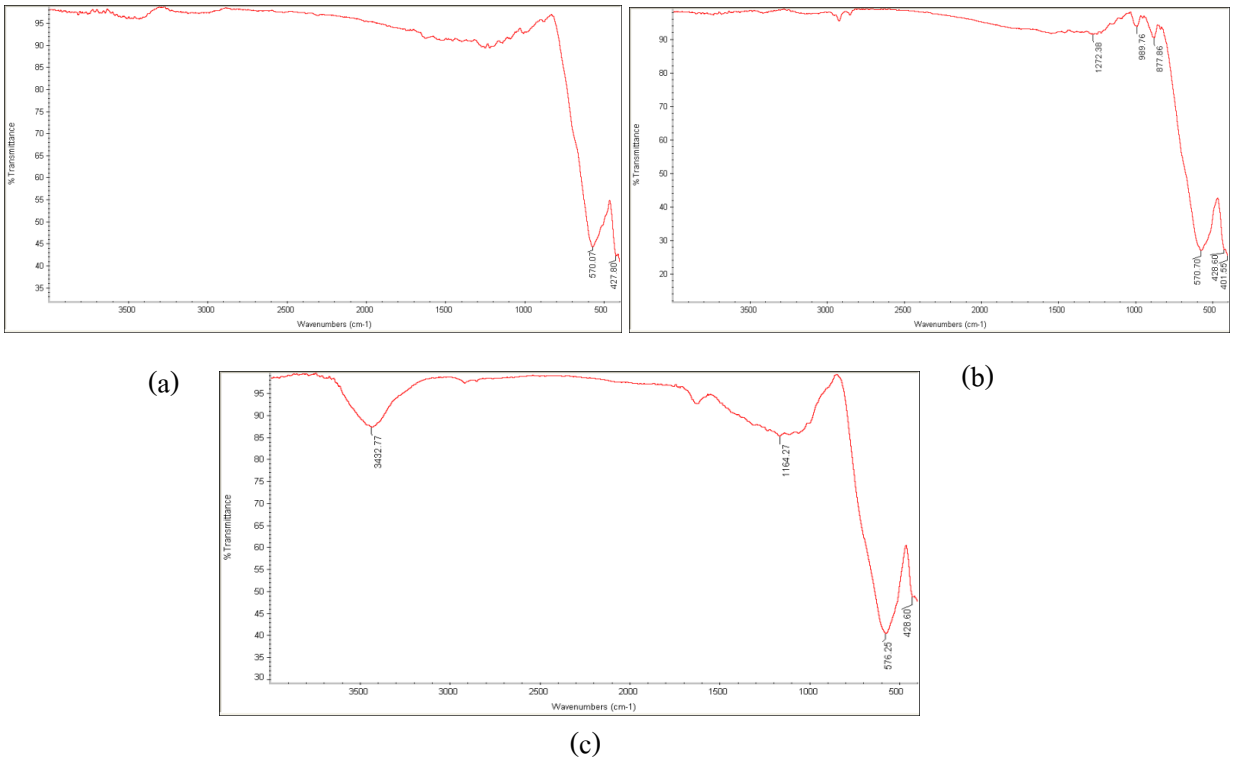

(a) (b) (c)

Figure 10 Displays the FTIR for the ferrite component $Mg_{1-x}Cu_xFe_2O_4$ whitout plasma exposure, with (a) x = 0, (b) x = 0.3, (c) x = 0.7.

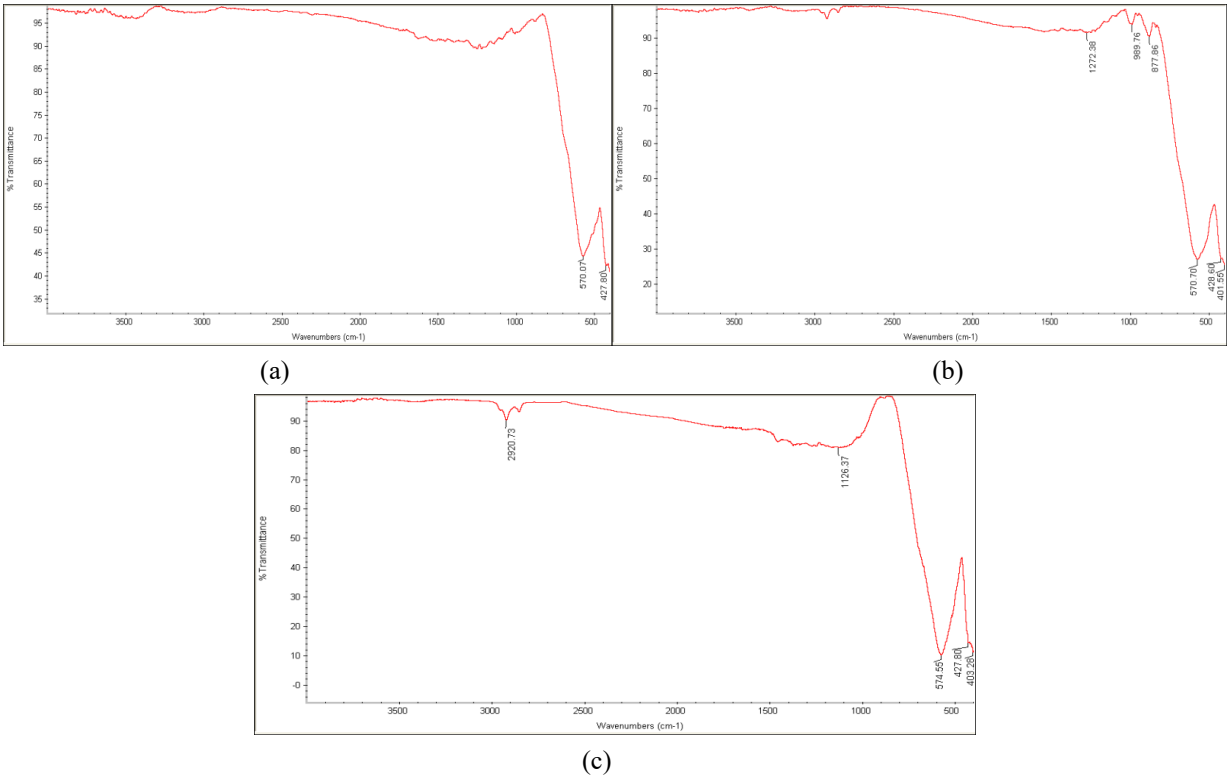

Figure 11 Displays the FTIR for the ferrite component $Mg_{1-x}Cu_xFe_2O_4$ following plasma exposure, with (a) x = 0, (b) x = 0.3, (c) x = 0.7.

Conclusions

For the purpose of studying Cu-substitution's impact on the material's structural and magnetic properties, $Mg_{1-x}Cu_xFe_2O_4$ nanoferrites with different x ratios were prepared using the sol-gel procedure. The $Mg_{1-x}Cu_xFe_2O_4$ ferrite crystal size shrinks as the Cu concentration increases. To expose the produced samples with relation to plasma. The ferrite combination showed a reduction in crystal size as copper content increased. Particle size variation was shown by the FE-SEM analysis grain size distribution and semi-spherical shapes in $MgFe_2O_4$ nanoferrites. Exposure to plasma causes a considerable change in the crystal's form and size, resulting in a heterogeneous and non-spherical structure. Prior to plasma exposure, the complex $Mg_{1-x}Cu_xFe_2O_4$ experienced fluctuations in magnetic saturation, affecting the force coercive by raising the ratio (x) owing to differences in crystalline magnetism. Exposing the compound $Mg_{1-x}Cu_xFe_2O_4$ to plasma resulted in higher Ms, Mr and Hc values than the unexposed samples. The escalation was caused by increased temperatures on the surface of ferrite samples when exposed to microwave plasma. Both materials' infrared spectra show 2 prominent absorption bands, according to FTIR measurements taken before they were exposed to the plasma (metal-oxygen bonds). Both strips expand when the 2 compounds are exposed to plasma. In future, ferrite may be synthesised via co-precipitation, and its characteristics are examined using SEM and EDX.

Acknowledgements

The authors would like to acknowledge the support from the Department of Physics, College of Science, University of Babylon, Iraq for assisting in sample preparation throughout this work.

Declaration of Generative AI in Scientific Writing

The authors acknowledge the utilisation of generative AI tools (e.g., QuillBot and Grammar Checker) in the production of this manuscript, with a particular emphasis on language revision and grammar correction. No content generation or data interpretation was performed by AI. The authors take full

responsibility for the content and conclusions of this work.

CRediT author statementWidhya

Alyaa: Conceptualization, Methodology, Supervision, Validation, Funding acquisition, and Writing –original draft.

Ibtesam Omran Radi: Data curation, Validation, Formal analysis, and Visualization.

Faten D.Mirjan: Data curation, Formal analysis, Investigation, Validation.

References

[1] KM Srinivasamurthy, VJ Angadi, SP Kubrin, S Matteppanavar, DA Sarychev, PM Kumar, HW Azale and B Rudraswamy. Tuning of ferrimagnetic nature and hyperfine interaction of Ni^{2+}doped cobalt ferrite nanoparticles for power transformer applications. *Ceramics International* 2018; **44(8)**, 9194-9203.

[2] AI Abda, AL Abedb and DS Ahmeda. Effect of variation of zinc content and sintering temperature on structural properties of some ferrite materials. *Acta Physica Polonica Series A* 2018, **134(1)**, 139-144.

[3] S Khorrami, F Gharib, G Mahmoudzadeh, SS Sepehr, SS Madani1, N Naderfar and S Manie. Synthesis and characterization of nanocrystalline spinel zinc ferrite prepared by sol-gel auto-combustion technique. *International Journal of Nano Dimension* 2019; **1(3)**, 221-224.

[4] S Tippireddy, F Azough, A Bhui, I Mikulska, R Freer, K Biswas, P Vaqueiro and AV Powell. Enhancement of thermoelectric properties of $CuFeS_2$ through formation of spinel-type microprecipitates. *Journal of Materials Chemistry A* 2023, **11(42)**, 22960-22970.

[5] D Varshney, K Verma and A Kumar. Substitutional effect on structural and magnetic properties of $A_xCo_{1-x}Fe_2O_4$ (A = Zn, Mg and x = 0.0, 0.5) ferrites. *Studies in Physical and Theoretical Chemistry* 2011; **1006**, 447-452.

[6] D Bokov, AT Jalil, S Chupradit, W Suksatan, MJ Ansari, IH Shewael, GH Valiev and E Kianfar. Nanomaterial by sol-gel method: Synthesis and application. *HindawiAdvances in Materials Science and Engineering* 2021; **2021**, 1-21.

[7] MS Khandekar, RC Kambale, SS Latthe, JY Patil, PA Shaikh, N Hur and SS Suryavanshi. Role of fuels on intrinsic and extrinsic properties of $CoFe_2O_4$ synthesized by combustion method. *Materials Letters* 2011, **65(19-20)**, 2972-2974.

[8] J Yuennan, N Muensit, N Tohluebaji, W Chailad, L Yang, N Sukhawipat, GA Ashraf and P Channuie. Tailoring dielectric properties and crystallinity in poly(vinylidene fluoride-co-hexafluoropropylene) nanocomposites via iron (III) chloride hexahydrate incorporation. *Scientific Reports* 2025; **15(1)**, 17810.

[9] J Balavijayalakshmi, N Suriyanarayanan and R Jayaprakash. Role of copper on structural, magnetic and dielectric properties of nickel ferrite nano particles. *Journal of Magnetism and Magnetic Materials* 2015; **385**, 302-307.

[10] M Ismael and M Wark. A simple sol-gel method for the synthesis of Pt co-catalyzed spinel-type $CuFe_2O_4$ for hydrogen production; the role of crystallinity and band gap energy. *Fuel* 2024; **359**, 130429.

[11] D Bharti, K Mukherjee and S Majumder. Wet chemical synthesis and gas sensing properties of magnesium zinc ferrite nano-particles. *Materials Chemistry and Physics* 2010; **120(2-3)**, 509-517.

[12] CD Lokhande, SS Kulkarni, RS Mane and SH Han. Copper ferrite thin films: Single-step non-aqueous growth and properties. *Journal of Crystal Growth* 2017; **303(2)**, 387-390.

[13] DT Rahardjo, S Budiawanti, S Suharno, R Suryana, A Supriyanto and B Purnama. Decreasing of magnetic saturation of yttrium doped cobalt ferrite prepared by the sol-gel auto-combustion. *Trends in Science* 2024; **21(4)**, 7320.

[14] A Farheen and R Singh. Effect of hydrothermal annealing on structure and magnetic properties of rf sputtered Mn-Zn ferrite thin films. *Materials Research Express* 2019; **6**, 114001.

[15] BS Mahdi and IO Radi. Ab-initio restricted hartree-fock formalism using for calculations electronic structure of grey tin nanocrystals crystal. *Chemical and Process Engineering Research* 2013; **17**, 1-10.

[16] M Ansari, A Bigham and HA Ahangar. Super-paramagnetic nanostructured CuZnMg Mxed

spinel ferrite for bone tissue regeneration. *Materials Science and Engineering: C* 2019; **105**, 110084.

[17] A.H Abbas, MA Al-Shareefi and AA Khadyair. Influence of exposure $Cd_{1-x}Mg_x$ Fe_2O_4 compound by RF plasma. *Journal of University of Babylon for Pure and Applied Sciences* 2023; **31(2)**, 226-236.

[18] T.M Hammad, S Kuhn, AA Amsha, NK Hejazy and R Hempelmann. Comprehensive Study of the impact of Mg^{+2} doping on optical, structural, and magnetic properties of copper nanoferrites. *Journal of Superconductivity and Novel Magnetism* 2020; **33(14)**, 3065-3075.

[19] A.H Abbas Aziz, MA Al-Shareefi and AA Khadyair. Modulating magnetic properties of ferrite $Cu_{1-X}Mg_XFe_2O_4$ via RF plasma exposure: Effects of magnesium concentration. *Journal of Composite and Advanced Materials* 2023; **33(4)**, 267-274.

[20] M Desai, J Dash, I Samajdar, N Venkataramani, S Prasad, P Kishan and N Kumar. A TEM study on lithium zinc ferrite thin films and the microstructure correlation with the magnetic properties. *Journal of Magnetism and Magnetic Materials* 2011; **231(1)**, 108-112.

[21] TM Hammad and NK Hejazy. Structural, morphological, optical and magnetic properties of $Cu_{1-x}Ni_xFe_2O_4$ nanoferrites. *International Journal of Applied Science and Research* 2021; **4(6)**, 153-170.

[22] O Mounkachi, M Hamedoun, M Belaiche, A Benyoussef, R Masrour, HE Moussaoui and M Sajieddine. Synthesis and magnetic properties of ferrites spinels $Mg_xCu_{1-x}Fe_2O_4$. *Physica B: Condensed Matter* 2012; **407(1)**, 27-32.

[23] A Safari, K Gheisari and M Farbod. The effect of plasma arc discharge process parameters on the properties of nanocrystalline $(Ni,Fe)Fe_2O_4$ ferrite: Structural, magnetic and dielectric studies. *Journal of Magnetism and Magnetic Materials* 2022; **541**, 168536.

[24] HS Jabr and RH Abdali. The effect of nitrogen on the structural and electronic properties of graphene sheet using density functional theory. *Acta Scientifica Naturalis* 2022: **9(2)**, 1-9.

[25] W Fang, L Yu and L Xu. Preparation, characterization and photocatalytic performance of heterostructured CuO-ZnO-loaded composite nanofiber membranes. *Beilstein Journal of Nanotechnology* 2020; **11(1)**, 631-650.

[26] R Ramadan and MM El-MasryBarka. Efect of (Co and Zn) doping on structural, characterization and the heavy metal removal efciency of $CuFe_2O_4$ nanoparticles. *Journal of the Australian Ceramic Society* 2024; **60(5)**, 1-16.